Collective oscillations in supernova neutrinos: onset and beyond

Arka Banerjee
under the guidance of Prof. Amol Dighe

Neutrino-neutrino interactions in dense neutrino streams, like those emitted by a core-collapse supernova, lead to self-induced neutrino flavor conversions. While this is a nonlinear phenomenon, we point out in the first part of the report that the onset of these conversions can be examined through a standard stability analysis of the linearized equations of motion. This technique allows for a systematic study of the onset conditions for collective flavor transformations, including the dependence on the neutrino density, energy spectrum, angular distribution, and matter density. In the second part, we look at the analytic solutions of the full non-linear equations for highly simplified spectra, and study how these solutions can explain various features seen in simulations such as large bipolar oscillations, and spectral splits.

I. INTRODUCTION

The study of supernova neutrinos has been an extremely active area of research, especially in the last three decades. Neutrino flavor oscillations in a supernova (SN) are strongly suppressed by matter effects [1] until the neutrinos pass through the usual MSW region [2–5] far out in the envelope of the collapsing star. However, neutrino-neutrino interactions [6, 7], through a flavor off-diagonal refractive index, can trigger self-induced flavor conversions [8–11]. This collective effect tends to occur between the neutrino sphere and the MSW region and can lead to strongly modified neutrino spectra, showing features such as spectral swaps and splits [12–17]; for a review see Ref. [18]. The overall scenario, supported by heuristic arguments and numerical examples, is that deep inside the SN core, the system performs "synchronized oscillations" with an extremely small amplitude, i.e. every neutrino remains essentially stuck in its initial flavor eigenstate. As the neutrinos stream outwards, there is a sharp onset radius where "bimodal" oscillations begin: Some ranges of modes start pendulum-like oscillations [11, 19–21], exchanging their flavor content with each other without affecting the flavor content of the overall system.

This scenario engenders a crucial simplification for the treatment of neutrino transport in SN simulations. At high densities, where neutrinos collide frequently, it is enough to solve the transport equations for each flavor separately, ignoring oscillations entirely. On the other hand, flavor conversions at larger distances can be treated ignoring neutrino collisions and absorption, i.e. as a pure propagation problem. So collisions and flavor oscillations are phenomena that are assumed to be taking place in different regions of the star and can be treated independently. When the radial distance where bimodal oscillations begin is far away from the SN core, this assumption is valid and the flavor conversions do not affect the SN dynamics. Recent studies dedicated to the SN accretion phase, under simplifying assumptions, once more confirm this picture [22, 23].

However, what is missing is a systematic approach to decide, without solving the equations of motion, if self-induced flavor conversions occur for given neutrino spectra (flavor-dependent energy and angular distribution), overall neutrino density, and matter density. Formal stability criteria exist only in the "single-angle approximation" where it is assumed that all neutrinos feel the same neutrino-neutrino refractive effect. In this case the analytic pendulum solution has been found and its existence and parameters can be calculated from the neutrino spectrum and density alone [17].

On the other hand, the current-current nature of the low-energy weak-interaction Hamiltonian implies that neutrinos in the background of an anisotropic neutrino flux experience a refractive effect that strongly depends on direction. For some energy spectra, these "multi-angle effects" have little impact, whereas in other cases they completely change the solution. In addition, the presence of ordinary matter causes a multi-angle suppression of the bimodal instability [28].

Although our problem is nonlinear and therefore would seem intractable, noting that an instability must occur in order for the onset to take place leads to a surprising simplification. In the dense SN matter well inside of the MSW region, the matter effect is so large that neutrino propagation eigenstates are essentially identical with flavor eigenstates. This means that in the weak-interaction basis, the flavor matrices of occupation numbers are almost perfectly diagonal. This allows us to linearize the equations of motion (EoMs) in terms of the small off-diagonal elements, as long as we are at a distance large compared to the size of the SN core. An instability is equivalent to some of these small elements starting to grow exponentially.

In Sec. II, we try to undertsand heuristically the origins of the neutrino-neutrino interaction term and write the effective Hamiltonian under which the neutrinos evolve. We also briefly survey the current results in the field. In Sec. III we derive the linearized equations of motion at a large distance from the neutrino source in the two-flavor case, with an azimuthally symmetric neutrino emission. In Sec. IV, we present the stability analysis in the single-angle approximation, and illustrate it in Sec. V with the examples of box spectra where the results may be understood analytically. Sec. VI and VII demonstrate how

the single-angle results are modified by the inclusion of multi-angle effects and matter effects. The latter one also analyzes a realistic SN spectrum using the insights obtained from the box spectra. In Sec. VIII, we point out a novel consequence of multi-angle effects for small lepton asymmetry and small matter effects. In Sec. IX, we solve the full non-linear equations of motion for the simple asymmetric two-box spectrum under the single-angle assumption in a fixed background. Sec. X looks at how these solutions should be modified so as to describe the non-linear oscillations when the background changes adiabatically. In Sec. XI we conclude with a brief summary of our findings and an outlook on future directions.

II. NEUTRINO-NEUTRINO INTERACTION TERM

When the neutrino passes through a background with N_s number of scatterers, the forward scattering amplitudes add up coherently and the effective cross-section is proportional to N_s^2. For other processes, the effective cross-section is proportional to N_s. Therefore, in sufficiently dense backgrounds, we can concentrate only on the forward scattering events. For the sake of simplicity, we will work throughout with two active neutrino flavors, e and x, instead of three. While there are new and subtle effects of introducing the third flavor, most of the arguments and results derived in this project can be extended to the more realistic case of three neutrinos without major modifications.

We consider the case of a large number of neutrinos passing through a small region of space. For better understanding, let us tag one of the neutrinos as a test neutrino and the rest as background neutrinos. As the test neutrino moves through the background, there are two possible tree level Feynman diagrams which can lead to coherent forward scattering.

If the test neutrino scatters off a background neutrino of the same flavor, then there is no flavor conversion, as seen in Figs. 1(b) and 1(c). Even if the the test neutrino and background flavors are different, $t-$channel is diagonal in the flavor basis and does not lead to flavor conversion, as can be seen in 1(a). However, the $u-$channel diagram, shown in 1(d), is not diagonal in the flavor basis and leads to the collective flavor oscillations. As a concrete example, we consider a ν_e scattering off a background of ν_x. Then the original electron neutrino exchanges momentum with one of the neutrinos in the background: ν_e goes into the background whereas one of the neutrinos from the background picks up the momentum of the ν_e. One such process can be represented as

$$|e\rangle + |x, x, ...x\rangle \rightarrow |x\rangle + |e, x, ...x\rangle \tag{1}$$

Therefore,we have to include the amplitudes of all such exchange with the other components of the background.

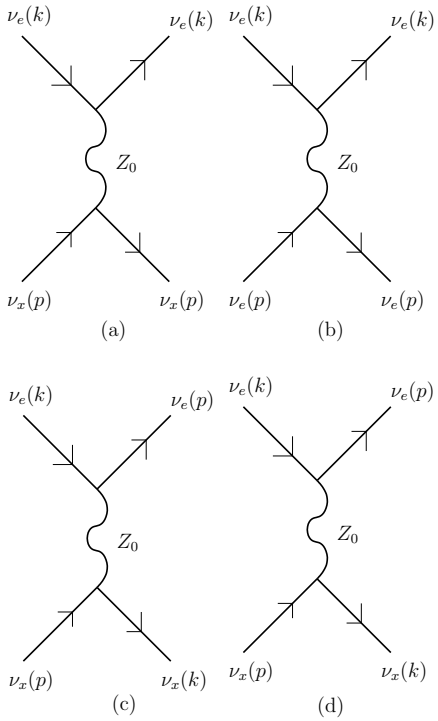

FIG. 1: Tree-level Feynman diagrams contributing to forward scattering. The first three diagrams are all diagonal in the flavor basis. The last diagram is the one leading to off-diagonal terms in the Hamiltonian.

Because of the presence of these new interactions, terms have to be added to the total Hamiltonian. These new interactions are neutral current ones mediated by the Z boson. The typical energies of the neutrinos emitted near the core of supernovae is of the order $10MeV$. Therefore, we are in the regime where we can safely use the four-Fermi interactions for our calculations rather than the full-blown electroweak calculation. According to the four-Fermi theory, the neutrino-neutrino neutral current interaction Hamiltonian is given by

$$H_{NC}^{ij} = \frac{G_F}{\sqrt{2}} \left(\bar{\nu}_{iL}\gamma^{\mu}\nu_{iL}\right)\left(\bar{\nu}_{jL}\gamma_{\mu}\nu_{jL}\right) \tag{2}$$

where the indices i, j stand for neutrino species and L denotes the left-handed chirality. Before calculating the potential arising out of this term in the Hamiltonian, let us first set down some useful notation. In the flavor basis, the wavefunction of a neutrino is given by

$$\psi_{\nu} = \begin{pmatrix} \nu_e \\ \nu_x \end{pmatrix} \tag{3}$$

where we have assumed that the wavefunction is correctly normalized. From the above wavefunction, the density matrix operator of all neutrinos at any given point with momentum $\mathbf{k}$ can be written as

$$\varrho_{E,\mathbf{v}} = n_{\nu}(E) \begin{pmatrix} |\nu_e|^2 & \nu_e\nu_x^* \\ \nu_e^*\nu_x & |\nu_x|^2 \end{pmatrix} \tag{4}$$

where $n_\nu(E)$ is the local density of neutrinos summed over all species. The velocity vector $\mathbf{v}$ with $|\mathbf{v}| = 1$ describes the direction of motion

Since we are looking only at forward scattering amplitudes, where momenta of the interacting neutrinos are either conserved or exchanged, we can write the new potential term in the Hamiltonian for neutrinos as

$$H_{\nu\nu} = \frac{G_F}{\sqrt{2}} \times \tag{5}$$
$$\begin{pmatrix} \int dE d\mathbf{v}\, [\bar{\nu}_{e,E',\mathbf{v}'}\gamma^\mu(1-\gamma_5)\nu_{e,E',\mathbf{v}'}]\,[\bar{\nu}_{i,E,\mathbf{v}}\gamma_\mu(1-\gamma_5)\nu_{i,E,\mathbf{v}}] & \int dE d\mathbf{v}\, [\bar{\nu}_{e,E'\mathbf{v}'}\gamma^\mu(1-\gamma_5)\nu_{e,E,\mathbf{v}}]\,[\bar{\nu}_{x,E,\mathbf{v}}\gamma_\mu(1-\gamma_5)\nu_{x,E',\mathbf{v}'}] \\ \int dE d\mathbf{v}\, [\bar{\nu}_{x,E',\mathbf{v}'}\gamma^\mu(1-\gamma_5)\nu_{x,E,\mathbf{v}}]\,[\bar{\nu}_{e,E,\mathbf{v}}\gamma_\mu(1-\gamma_5)\nu_{e,E',\mathbf{v}'}] & \int dE d\mathbf{v}\, [\bar{\nu}_{x,E',\mathbf{v}'}\gamma^\mu(1-\gamma_5)\nu_{x,E',\mathbf{v}'}]\,[\bar{\nu}_{i,E,\mathbf{v}}\gamma_\mu(1-\gamma_5)\nu_{i,E,\mathbf{v}}] \end{pmatrix}$$

The momentum integral in (5) is over all background neutrinos and the index i runs over e, μ. We see that the diagonal terms are those where the momentum of the incoming particle remains unchanged, whereas the off-diagonal terms are the ones where the incoming neutrino exchanges momentum with the background neutrino.

Upon explicitly evaluating the matrix elements, and throwing away terms proportional to the identity matrix, the neutrino interaction Hamiltonian reads [7]

$$H_{\nu\nu} = \frac{1}{2}\begin{pmatrix} B & B_{ex} \\ B^*_{ex} & -B \end{pmatrix} \tag{6}$$

where

$$B = \sqrt{2}G_F \int dE\; d\mathbf{v}(1-\mathbf{v}.\mathbf{v}')\,[(\varrho_{E,\mathbf{v}})_{ee} - (\varrho_{E,\mathbf{v}})_{xx}] \tag{7}$$

$$B_{ex} = 2\sqrt{2}G_F \int dE\; d\mathbf{v}(1-\mathbf{v}.\mathbf{v}')\,[(\varrho_{E,\mathbf{v}})_{ex}] \tag{8}$$

A. Effective Hamiltonian

We write the EoMs in terms of 2×2 matrices of occupation numbers [7, 30]. As described in the last section, we denote these matrices by $\varrho_{E,\mathbf{v}}$, where the velocity vector $\mathbf{v}$ with $|\mathbf{v}| = 1$ describes the direction of motion and the energy E is taken to be positive for neutrinos and negative for antineutrinos. Also, while the diagonal entries are equal to the occupation numbers for neutrinos, they are the negative occupation numbers for antineutrinos. Our choice of signs, however, allows us to include neutrinos and antineutrinos on the same footing and we will never have to distinguish between them: The antineutrino spectrum is simply a continuation of the neutrino spectrum to negative energies. In the language of flavor polarization vectors, our convention agrees with the neutrino flavor isospin construction [12].

The EoMs for the time evolution in a homogeneous medium are

$$\mathrm{i}\partial_t \varrho_{E,\mathbf{v}} = [\mathsf{H}_{E,\mathbf{v}}, \varrho_{E,\mathbf{v}}]\,. \tag{9}$$

We use sans-serif letters for matrices in flavor space. The Hamiltonian matrix is

$$\mathsf{H}_{E,\mathbf{v}} = \frac{\mathsf{M}^2}{2E} + \sqrt{2}\,G_\mathrm{F}\mathsf{N}_\ell + \sqrt{2}\,G_\mathrm{F}\int_{-\infty}^{+\infty} dE' \int d\mathbf{v}'\,\frac{E'^2}{(2\pi)^3}\,\varrho_{E',\mathbf{v}'}(1-\mathbf{v}\cdot\mathbf{v}') \tag{10}$$

where M^2 is the neutrino mass-squared matrix and N_ℓ the matrix of net charged lepton densities which in the flavor basis is $\mathsf{N}_\ell = \mathrm{diag}(n_e - n_{\bar{e}}, n_x - n_{\bar{x}})$. In an isotropic medium, the $\mathbf{v}\cdot\mathbf{v}'$ term drops out and the neutrino-neutrino term has the same structure as the matter term: The phase-space integral over $\varrho_{E,\mathbf{v}}$ amounts to the difference between neutrino and antineutrino densities.

B. Summary of recent collective neutrino oscillations results

To understand the work done in this report in its proper context, we provide a brief survey into the relevant results that can be found in the literature. These results have been obtained under different approximations and in various regimes of the parameter space of matter effect and neutrino densities. Often, they seem to contradict each other, and have led to confusion over how to interpret the findings. These seemingly desultory results motivate the need for a consistent formalism which would allow us to explain all of them within its framework.

First, we look at studies which were done under the single-angle approxiamtion, and the results obtained therein:

- For a spectrum to perform collective oscillations in inverted hierarchy, it should have a positive spectral. For normal hierarchy, the spectrum should have a negative crossing to perform collective oscillations [17]. If a spectrum has more than one such crossing, there exists an instability corresponding to each.
- Deep inside the SN, where neutrino density is very high, neutrinos perform synchronized oscillations

with a very small amplitude: flavor oscillations are basically suppressed in this region [10]. However, numerical studies with a Fermi-Dirac spectrum showed no such synchronization regime [27].

- In the region where the neutrino density is lower, there exist pendular oscillations which cause large flavor conversions amongst various modes, without changing the overall flavor content [19].
- When the background neutrino deinsity falls off as the neutrinos stream out of the SN, these pendular modes become splits in the neutrino spectrum [13].

Next, we look at results from multi-angle studies:

- Collective oscillations are suppressed by multi-angle effects of neutrinos themselves. Adding normal matter to the system does not change the onset of collective oscillations [27].
- At extremely high matter densities collective oscillations are completely suppressed [22].
- For spectra with low lepton-number asymmetry, instabilities exist even for single-crossed spectra in both hierarchies [25].

III. LINEARIZED EQUATIONS OF MOTION

A. Azimuthally symmetric neutrino emission

We now return to the EoMs, and make certain simplifying assumptions that will help us to investigate the onset of collective oscillations analytically. Henceforth we assume azimuthal symmetry around some preferred direction, usually the radial direction in the SN case. The azimuthal integration provides

$$1 - \mathbf{v}\cdot\mathbf{v}' \to 1 - v\cdot v' \,, \tag{11}$$

where v and v' are the components of $\mathbf{v}$ and $\mathbf{v}'$, respectively, along the symmetry direction. Thus $v = \cos\vartheta$ with ϑ the trajectory angle relative to the symmetry direction.

We introduce an arbitrary sphere with radius R that we call neutrino sphere where we specify the inner boundary condition for neutrinos that are assumed to stream only outward. Every angular mode is described by its emission angle ϑ_R relative to the radial direction at that sphere (Fig. 3 of Ref. [18]) in terms of the variable $u = \sin^2\vartheta_R$ which lies in the range $0 \le u \le 1$. The u variable has the property that the modes are uniformly distributed on $0 \le u \le 1$ if the emission at the neutrino sphere is isotropic into space in analogy to black body emission.

At radius r, the radial velocity of a mode with angular label u is

$$v_{u,r} = \sqrt{1 - \frac{R^2}{r^2}\,u}\,. \tag{12}$$

In analogy to Ref. [25] we introduce the matrices

$$\Phi_{E,u,r} = \frac{r^2E^2}{2\pi}\,\varrho_{E,u,r}\,, \tag{13}$$

where we have included a factor $4\pi r^2$, so that the integrated quantity

$$\Phi_r = \int_{-\infty}^{+\infty} dE \int_0^1 du\,\Phi_{E,u,r} \tag{14}$$

represents the flux through a sphere of radius r whose trace is conserved.

The EoMs for the flux matrices as a function of radial coordinate are

$$\mathrm{i}\partial_r\Phi_{E,u,r} = [\mathsf{H}_{E,u,r}, \Phi_{E,u,r}] \tag{15}$$

with the Hamiltonian

$$\begin{aligned}\mathsf{H}_{E,u,r} &= \left(\frac{\mathsf{M}^2}{2E} + \sqrt{2}\,G_{\rm F}\mathsf{N}_\ell\right)\frac{1}{v_{u,r}} \\ &+ \frac{\sqrt{2}\,G_{\rm F}}{4\pi r^2}\int_0^1 du'\left(\frac{1}{v_{u,r}v_{u',r}} - 1\right)\Phi_{u',r}\,,\end{aligned} \tag{16}$$

where $\Phi_{u,r} = \int_{-\infty}^{+\infty} dE\,\Phi_{E,u,r}$.

B. At a large distance from source

We are interested in the evolution far away from the neutrino sphere where the flavor conversions are expected to begin. Therefore, we use the expansion

$$v_{u,r}^{-1} = 1 + \frac{u}{2}\,\frac{R^2}{r^2}\,. \tag{17}$$

Moreover, we introduce the dimensionless matrices $\mathsf{L} = \mathsf{N}_\ell/(n_e - n_{\bar e})$ and $\mathsf{F}_{E,u,r} = \Phi_{E,u,r}/\Phi_{\bar\nu_e}(R)$. Note that we normalize the charged-lepton density to the local net electron density, whereas the neutrino flux matrices are normalized to the total $\bar\nu_e$ flux at the neutrino sphere. If we use the flavor basis, with these normalizations we have $\mathsf{L}^{ee} = 1$ and $\int_{-\infty}^0 dE\int_0^1 du\,\mathsf{F}^{ee}_{E,u,r} = -1$ for all r where oscillations have not yet begun.

We also introduce the coefficients with dimension of inverse energy

$$\begin{aligned}\tilde\lambda_r &= \sqrt{2}\,G_{\rm F}\left[n_e(r) - n_{\bar e}(r)\right]\,, \\ \mu_R &= \frac{\sqrt{2}\,G_{\rm F}\Phi_{\bar\nu_e}(R)}{4\pi R^2}\,.\end{aligned} \tag{18}$$

In terms of these coefficients, we have

$$\mathrm{i}\partial_r\mathsf{F}_{E,u,r} = [\mathsf{H}_{E,u,r}, \mathsf{F}_{u,r}]\,, \tag{19}$$

with

$$\begin{aligned}\mathsf{H}_{E,u,r} &= \left(\frac{\mathsf{M}^2}{2E} + \tilde\lambda_r\mathsf{L}\right)\left(1 + \frac{u}{2}\,\frac{R^2}{r^2}\right) \\ &+ \mu_R\,\frac{R^4}{r^4}\int_0^1 du'\,\frac{u+u'}{2}\,\mathsf{F}_{u',r}\end{aligned} \tag{20}$$

as the Hamiltonian at the lowest-order in (R/r), with $\mathsf{F}_{u,r} = \int_{-\infty}^{+\infty} dE\, \mathsf{F}_{E,u,r}$. The first line on the right hand side of Eq. (20) is the "vacuum plus matter" Hamiltonian $\mathsf{H}^{\rm vac+mat}_{E,u,r}$ while the second line is the neutrino-neutrino Hamiltonian $\mathsf{H}^{\nu\nu}_{E,u,r}$.

We introduce the variable $\omega = |\Delta m^2|/2E$. Note that since E is taken to be negative for antineutrinos, they are represented by negative ω values.

Since the trace of the Hamiltonian does not contribute to the time evolution, we write

$$\begin{aligned} \frac{\mathsf{M}^2}{2E} &= \pm\frac{\omega}{2}\begin{pmatrix} \cos 2\theta & \sin 2\theta \\ -\sin 2\theta & -\cos 2\theta \end{pmatrix}, \\ \tilde{\lambda}_r \mathsf{L} &= \frac{\tilde{\lambda}_r}{2}\begin{pmatrix} 1 & 0 \\ 0 & -1 \end{pmatrix}, \end{aligned} \tag{21}$$

in the flavor basis, after removing a term proportional to the unit matrix. Here the $+(-)$ sign stands for inverted (normal) hierarchy. In the following discussion, we shall consider inverted hierarchy. For obtaining results with normal hierarchy, we'll have to multiply the ω term by a factor of -1.

The flux matrices at the neutrino sphere are

$$\mathsf{F}_{\omega,u,R} = \begin{pmatrix} \phi^e_{\omega,u} & 0 \\ 0 & \phi^x_{\omega,u} \end{pmatrix}, \tag{22}$$

where the $\phi_{\omega,u}$ are differential fluxes in the variables ω and u.

The normalization of F used here implies that $\int_{-\infty}^{0} d\omega \int_0^1 du\, \phi^e_{\omega,u} = -1$. Note that $\phi_{\omega,u}$ for antineutrinos ($\omega < 0$) corresponds to the negative of their occupation numbers.

Finally, in the flavor basis we write

$$\mathsf{F}_{\omega,u,r} = \frac{\mathrm{Tr}\,\mathsf{F}_{\omega,u,r}}{2} + \frac{g_{\omega,u}}{2}\,\mathsf{S}_{\omega,u,r}\,, \tag{23}$$

where $g_{\omega,u} = \phi^e_{\omega,u} - \phi^x_{\omega,u}$ is the usual difference spectrum, except that it is now also differential with regard to the direction variable u. The initial conditions at the neutrinosphere for the Hermitian matrix $\mathsf{S}_{\omega,u,r}$ are

$$\mathsf{S}_{\omega,u,R} = \begin{pmatrix} 1 & 0 \\ 0 & -1 \end{pmatrix}, \tag{24}$$

and the EoMs satisfied by it are

$$\mathrm{i}\partial_r \mathsf{S}_{\omega,u,r} = [\mathsf{H}_{E,u,r}, \mathsf{S}_{\omega,u,r}] \tag{25}$$

with the neutrino-neutrino part of the Hamiltonian

$$\mathsf{H}^{\nu\nu}_{\omega,u,r} = \mu_r \int_0^1 du'\,(u+u') \int_{-\infty}^{+\infty} d\omega'\, \frac{g_{\omega'u'}}{2}\,\mathsf{S}_{\omega',u',r}\,. \tag{26}$$

Here

$$\mu_r = \mu_R\,\frac{R^4}{2r^4}\,. \tag{27}$$

The effective neutrino-neutrino interaction energy declines with r^{-4}.

C. In a co-rotating frame

We go to a rotating frame where the common matter term drops out and where the vacuum term oscillates quickly, averaging the off-diagonal term to zero [28]. Moreover, in the large-r limit we ignore a small radius-dependent shift of ω. Then we find

$$\mathsf{H}^{\rm vac+mat}_{\omega,u,r} = \frac{\omega + u\lambda_r}{2}\begin{pmatrix} 1 & 0 \\ 0 & -1 \end{pmatrix}, \tag{28}$$

where

$$\lambda_r = \tilde{\lambda}_r\,\frac{R^2}{2r^2} = \sqrt{2}\,G_{\rm F}\,[n_e(r) - n_{\bar{e}}(r)]\,\frac{R^2}{2r^2} \tag{29}$$

encodes the effective matter effect.

Next we write the S matrices in components in the flavor basis

$$\mathsf{S}_{\omega,u,r} = \begin{pmatrix} s_{\omega,u,r} & S_{\omega,u,r} \\ S^*_{\omega,u,r} & -s_{\omega,u,r} \end{pmatrix}, \tag{30}$$

where $s_{\omega,u,r}$ is the r-dependent swap factor. It specifies how much the flavor content of the given mode has been swapped relative to the initial condition. We have the normalization $s^2_{\omega,u,r} + |S_{\omega,u,r}|^2 = 1$. Likewise,

$$\mathsf{H}_{\omega,u,r} = \begin{pmatrix} h_{\omega,u,r} & H_{\omega,u,r} \\ H^*_{\omega,u,r} & -h_{\omega,u,r} \end{pmatrix}. \tag{31}$$

Then the EoM for the off-diagonal component is

$$\mathrm{i}\partial_r S_{\omega,u,r} = 2\,(h_{\omega,u,r} S_{\omega,u,r} - s_{\omega,u,r} H_{\omega,u,r})\,. \tag{32}$$

The components of the Hamiltonian matrix are explicitly

$$\begin{aligned} h_{\omega,u,r} &= \frac{\omega + u\,\lambda_r}{2} \\ &\quad + \frac{\mu_r}{2}\int_0^1 du'\,(u+u') \int_{-\infty}^{+\infty} d\omega'\, g_{\omega'u'}\, s_{\omega',u',r}\,, \\ H_{\omega,u,r} &= \frac{\mu_r}{2}\int_0^1 du'\,(u+u') \int_{-\infty}^{+\infty} d\omega'\, g_{\omega'u'}\, S_{\omega',u',r}\,. \end{aligned} \tag{33}$$

In the absence of all interactions, the rotation-averaged EoM is

$$\mathrm{i}\partial_r S_{\omega,u,r} = \omega\, S_{\omega,u,r}\,, \tag{34}$$

implying the free precession solution

$$S_{\omega,u,r} = e^{-\mathrm{i}\omega(r-R)}\, S_{\omega,u,R}\,. \tag{35}$$

D. Small-amplitude expansion

Henceforth we drop the explicit subscript r to denote the r-dependence of all quantities. Moreover, we drop the limits of integration which are always as above. In the

small-amplitude case we have $s_{\omega,u} = 1$. This simplifies in particular the diagonal Hamiltonian term which is

$$h_{\omega,u} = \frac{\omega + u\,\lambda}{2} + \frac{\mu}{2}\int du'\,(u+u')\int d\omega'\,g_{\omega',u'}\,. \quad (36)$$

In the neutrino-neutrino term, the integral which involves $\int du' u' \ldots$ is a constant that does not depend on ω or u and therefore amounts to a shift of all frequencies, i.e. yet another rotating frame. Once more we can drop this term and are left with

$$h_{\omega,u} = \frac{\omega + u\,(\lambda + \epsilon\mu)}{2} \quad (37)$$

where

$$\epsilon = \int du\,d\omega\,g_{\omega,u} \quad (38)$$

quantifies the "asymmetry" or "total lepton number" of the neutrino spectrum, normalized to the total $\bar{\nu}_e$ flux.

The EoMs are then explicitly

$$\begin{aligned} \mathrm{i}\partial_r S_{\omega,u} &= [\omega + u(\lambda+\epsilon\mu)]\,S_{\omega,u} \\ &- \mu\int du'\,d\omega'\,(u+u')\,g_{\omega'u'}\,S_{\omega',u'}\,. \end{aligned} \quad (39)$$

This is the linearized form of the EoMs and provides the starting point for the stability analysis.

E. Eigenvalue equation

The stability analysis determines if the small quantities $S_{\omega,u}$ grow exponentially with time (or equivalently, with r). This is achieved by writing $S_{\omega,u}$ as

$$S_{\omega,u} = Q_{\omega,u}\,e^{-\mathrm{i}\Omega r}\,, \quad (40)$$

where both $Q_{\omega,u}$ and Ω are in general complex numbers. A real solution for Ω would imply precession modes, possibly with frequncies depending on ω and u. A complex solution $\Omega \equiv \gamma + i\kappa$, with $\kappa > 0$, would indicate a exponentially increasing $S_{\omega,u}$, i.e., an instability. If $\kappa < 0$, one would have a exponentially decreasing solution, which will be undetectable in numerical solutions after a long time.

In terms of $Q_{\omega,u}$, the EoM becomes

$$(\omega + u\bar{\lambda} - \Omega)Q_{\omega,u} = \mu\int du'\,d\omega'\,(u+u')\,g_{\omega'u'}\,Q_{\omega',u'}\,, \quad (41)$$

where $\bar{\lambda} \equiv \lambda + \epsilon\mu$. This may be looked upon as an eigenvalue equation for $Q_{\omega,u}$ with the eigenvalue Ω.

IV. SINGLE-ANGLE STABILITY ANALYSIS

A. The consistency conditions

The single-angle approximation, which corresponds to the assumption that the neutrinos are emitted only at an angle $u = u_0$, makes the EoMs easier to analyze, at the same time reproducing many crucial features of the complete multi-angle analysis. We therefore first perform the stability analysis with this approximation. The next section will generalize it to the multi-angle scenario.

Since $u = u_0$, the term $u\bar{\lambda}$ in the EoM corresponds to a common precession for all modes. We therefore can go to a basis rotating with frequency $u_0\bar{\lambda}$, in which Eq. (39) becomes

$$\mathrm{i}\partial_r S_\omega = \omega\,S_\omega - 2u_0\mu\int d\omega'\,g_{\omega'}\,S_{\omega'}\,. \quad (42)$$

Requiring the solution to be of the form $S_\omega = Q_\omega\,e^{-\mathrm{i}\Omega r}$ gives

$$(\omega - \Omega)\,Q_\omega = 2u_0\mu\int d\omega'\,g_{\omega'}Q_{\omega'}\,. \quad (43)$$

This is the simplified form of the eigenvalue equation in Eq. (41).

For the l.h.s. of the eigenvalue equation to be independent of ω like the r.h.s. , we must have

$$Q_\omega \propto \frac{1}{\omega - \Omega}\,, \quad (44)$$

and therefore

$$\mu^{-1} = 2u_0\int d\omega\,\frac{g_\omega}{\omega - \Omega}\,. \quad (45)$$

For an instability, this equation should have a complex root $\Omega = \gamma + \mathrm{i}\kappa$. Then, splitting the equation into real and imaginary part, one obtains the two equations

$$(2u_0\mu)^{-1} = \int d\omega\,g_\omega\frac{\omega-\gamma}{(\omega-\gamma)^2+\kappa^2}\,. \quad (46)$$

$$0 = \int d\omega\,g_\omega\frac{\kappa}{(\omega-\gamma)^2+\kappa^2}\,, \quad (47)$$

Eqs. (46) and (47) are the conditions that must be simultaneously satisfied by γ and κ. These may be solved for a real γ and a positive κ^2. If a solution exists, it will correspond to an instability that will grow at the rate $e^{|\kappa|t}$.

B. Normal vs. inverted hierarchy

Recall that all our results have been obtained using inverted hierarchy. Going to normal hierarchy corresponds to changing Eq. (42) to

$$\mathrm{i}\partial_r\tilde{S}_\omega = -\omega\,\tilde{S}_\omega - 2u_0\mu\int d\omega'\,g_{\omega'}\,\tilde{S}_{\omega'}\,. \quad (48)$$

In terms of the solution S_ω of Eq. (42), the solution of this equation is given by

$$\tilde{S}_\omega(\mu, g_\omega) \;=\; S^*_\omega(\mu, -g_\omega) = S^*_\omega(-\mu, g_\omega)\,. \qquad (49)$$

Since S and S^* should have the same stability behavior, this implies that the stability conditions for normal hierarchy are the same as those for the inverted hierarchy with a change in the sign of g_ω or μ (not both at the same time).

V. SINGLE-ANGLE STABILITY ANALYSIS: EXAMPLES

In order to understand the behavior of the stability criteria, we shall first consider the toy example of a spectrum consisting of boxes of unit height, i.e. g_w only takes the values $0, \pm 1$. This makes the integral in Eq. (43) analytically calculable and as we shall see, Ω becomes the root of a polynomial whose degree depends on the number of boxes. As will be seen, the simplified box spectra already bring out some important features of the stability of the realistic SN spectra; viz. cutoff, saturation and multiple swaps.

A. Two-box spectrum

We start with a two-box spectrum, defined as

$$g_\omega = \begin{cases} -1 & -a < \omega < 0 \\ 1 & 0 < \omega < b \end{cases}\,. \qquad (50)$$

as shown in Fig. 2.

The consistency condition in Eq. (43) yields

$$\frac{\Omega^2}{(\Omega + a)(\Omega - b)} = \eta\,, \qquad (51)$$

where $\eta \equiv \exp^{-1/\mu}$. Note that $0 < \eta < 1$, while the limits $\mu \to \infty$ and $\mu \to 0$ correspond to $\eta = 1$ and $\eta = 0$, respectively.

The solutions are given by

$$\Omega = \frac{-(b-a)\eta \pm \sqrt{(b-a)^2\eta^2 - 4ab\eta(1-\eta)}}{2(1-\eta)}\,. \qquad (52)$$

The solutions have a non-vanishing imaginary part if the argument of the square-root is negative, i.e. for

$$0 < \eta < \eta_{synch} \equiv \frac{4ab}{(b+a)^2}\,. \qquad (53)$$

Here η_{synch} is the "synchronization strength," i.e. for a larger interaction strength the system is stuck in a stable position. If $0 < \eta < \eta_{synch}$, we find

$$\begin{aligned} \gamma &= -\frac{(b-a)\eta}{2(1-\eta)}\,, \\ \kappa &= \pm\frac{\sqrt{4ab\eta(1-\eta) - (b-a)^2\eta^2}}{2(1-\eta)}\,. \end{aligned} \qquad (54)$$

These solutions are shown in Fig. 2.

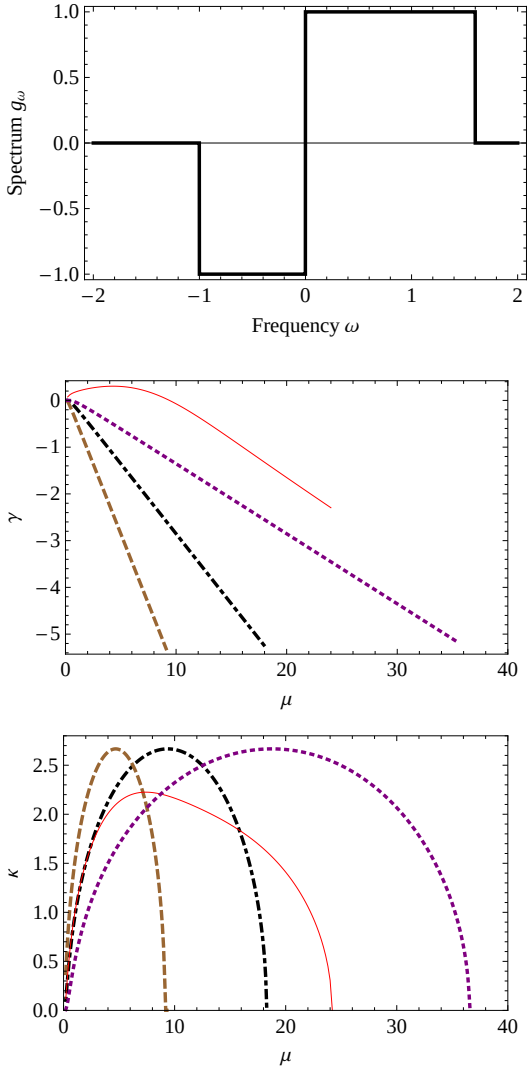

FIG. 2: A two-box spectrum, with $a = 1$ and $b = 1.6$, and its stability behavior in the single-angle approximation at different u_0 values. Brown (dashed) line: $u_0 = 1$, Black (dash-dotted) line: $u_0 = 1/2$, purple (dotted) line: $u_0 = 1/4$. Also shown is the multi-angle result (to be described in Sec. VII), with the red (solid) line.

B. Three-box spectrum

The three-box spectrum shows some additional features as compared to the two-box one. The three-box spectrum is defined as

$$g_\omega = \begin{cases} -1 & -a < \omega < 0 \\ 1 & 0 < \omega < b \\ -1 & b < \omega < c \end{cases}\,, \qquad (55)$$

and is shown in Fig. 3

The consistency condition in Eq. (43) yields

$$\frac{\Omega^2(\Omega - c)}{(\Omega + a)(\Omega - b)^2} = \eta\,, \qquad (56)$$

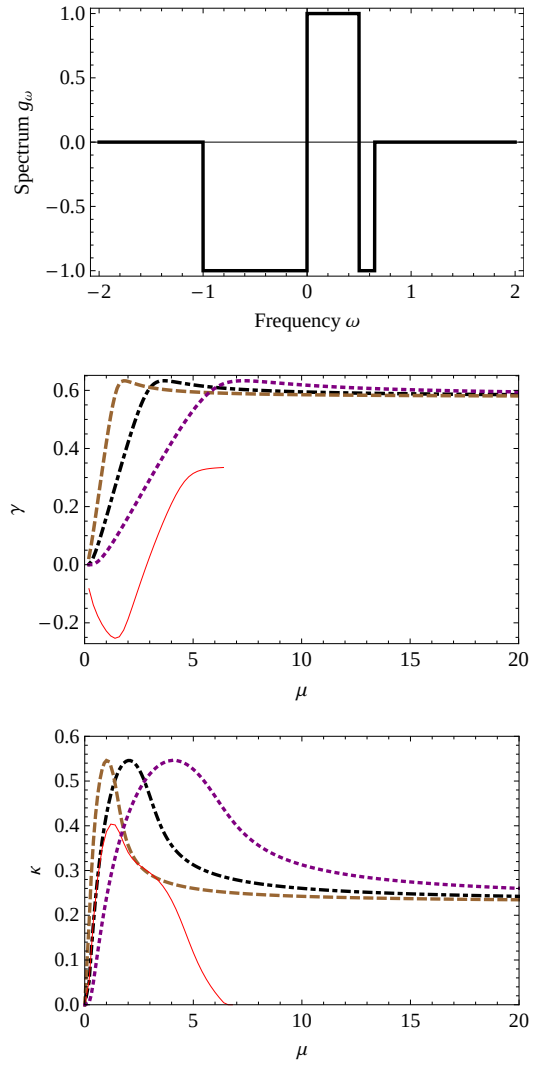

FIG. 3: A three-box spectrum, with $a = 1, b = 0.5, c = 0.6$, and its saturation behavior in the single-angle approximation at different u_0 values. Brown (dashed) line: $u_0 = 1$, Black (dash-dotted) line: $u_0 = 1/2$, purple (dotted) line: $u_0 = 1/4$. Also shown is the multi-angle result (to be described in Sec. VII), with the red (solid) line.

This can have three real roots, or a single real root and a pair of complex conjugate roots. The latter case corresponds to instability.

In order to study the stability at large μ, we look at the limit $\eta = 1$. In this limit, the cubic equation becomes a quadratic one:

$$(a - 2b + c)\Omega^2 + (b^2 - 2ab)\Omega + ab^2 = 0 \, . \qquad (57)$$

When the total lepton number is not zero, that is $2b - a - c \neq 0$, the solutions to this quadratic equation are

$$\Omega = \frac{2ab - b^2 \pm \sqrt{b(4ab + b^2 - 4ac)}}{2(a - 2b + c)} \, . \qquad (58)$$

- If $(4ab + b^2 - 4ac) > 0$ then the roots are both real, implying that the system is stable at extremely large μ values. We then get the same threshold behavior as was observed in the two-box case, similar to the one shown in Fig. 2.

- On the other hand, if $(4ab + b^2 - 4ac) < 0$, we can write $\Omega = \gamma \pm i\kappa$, with

$$\gamma = \frac{2ab - b^2}{2(a - 2b + c)} \, , \quad \kappa = \frac{\sqrt{b(4ac - b^2 - 4ab)}}{2(a - 2b + c)} \, . \qquad (59)$$

  Thus γ and κ stay finite even at arbitrarily large μ, and indeed, go to a constant, μ-independent value. The system is thus unstable even at large μ values. This saturation behavior, shown in Fig. 3, was absent in the two-box scenario. This would allow flavor conversions to start deep inside the core.

C. Four-box spectrum

The study of four-box spectra is relevant for some important reasons. First, the typical SN neutrino fluxes, where the luminosities of $\nu_e, \bar{\nu}_e$ and ν_x are comparable and their average energies follow a hierarchy $\langle E_{\nu_e} \rangle < \langle E_{\bar{\nu}_e} \rangle < \langle E_{\nu_x} \rangle$, the g_ω spectrum has three zero-crossings, which feature is reproduced by a four-box spectrum as can be seen in Fig. 4. Moreover, the consistency equation leads to a quartic equation in Ω, which may have none, one or even two complex roots, leading to interesting features in the stability analysis.

The spectrum is defined as

$$g_\omega = \begin{cases} -1 & -a < \omega < -b \\ 1 & -b < \omega < 0 \\ -1 & 0 < \omega < c \\ 1 & c < \omega < d \end{cases} \, . \qquad (60)$$

The self consistency condition in the linear approximation then gives

$$\frac{(\Omega + b)^2(\Omega - c)^2}{(\Omega + a)\Omega^2(\Omega - d)} = \eta \, . \qquad (61)$$

This can be rewritten as

$$\begin{aligned} (1 - \eta)\Omega^4 + (2b - 2c - a\eta + d\eta)\Omega^3 \\ + (b^2 - 4bc + c^2 + ad\eta)\Omega^2 \\ + (2bc^2 - 2b^2c)\Omega + b^2c^2 \;&=\; 0 \, . \end{aligned} \qquad (62)$$

We are interested in the limit $\eta = 1$. In this limit, the quartic equation reduces to a cubic equation with real coefficients. Hence we are guaranteed at least one real root. This implies that at large μ, we can have a maximum of one instability, corresponding to a possible pair of complex conjugate roots to this cubic equation. The existence of such a pair is determined by the value of the

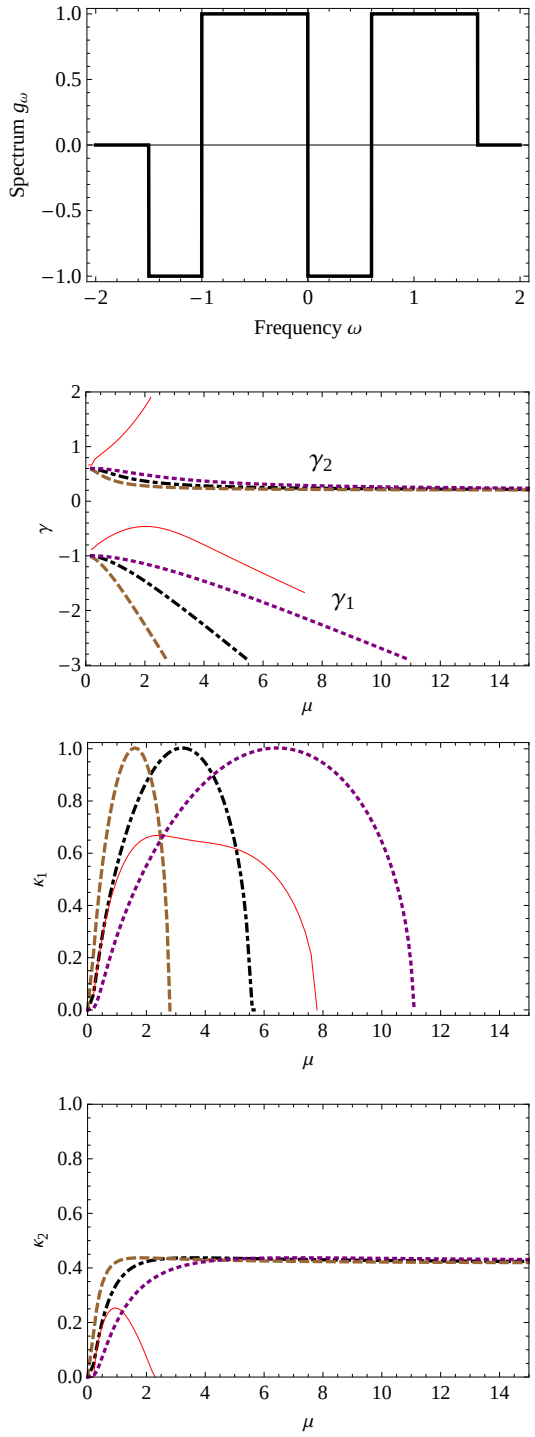

FIG. 4: A four-box spectrum, with $a = 1.5, b = 1.0, c = 0.6, d = 1.6$, and its stability behavior in the single-angle approximation at different u_0 values. Brown (dashed) line: $u_0 = 1$, Black (dash-dotted) line: $u_0 = 1/2$, purple (dotted) line: $u_0 = 1/4$. Also shown is the multi-angle result (to be described in Sec. VII), with the red (solid) line. The instability with higher γ is characterized by (γ_1, κ_1), while the other one is characterized by (γ_2, κ_2). Since $\Delta < 0$ at these parameters, one of the solutions shows the saturation behavior while the other shows cutoff behavior.

discriminant

$$\begin{aligned}\Delta &= b^2c^2[-27b^2c^2(a-2b+2c-d)^2 \\ &+ 32b(b-c)^3c(-a+2b-2c+d) \\ &- 36b(b-c)c(-a+2b-2c+d)(b^2-4bc+c^2+ad) \\ &+ 4(b-c)^2(b^2-4bc+c^2+ad)^2 \\ &- 4(b^2-4bc+c^2+ad)^3]\,. \end{aligned} \tag{63}$$

If $\Delta > 0$, all the roots are real and the system is stable. On the other hand, for $\Delta < 0$, we get an instability even for an extremely large μ value. Knowing the value of a, b, c, d, then, the stability or instability of the spectrum may be predicted.

A typical scenario is shown in Fig. 4. At low μ values, there are two instabilities, one of which shows a cutoff behavior, i.e. it vanishes for μ greater than a certain threshold value. The other instability, with $\gamma \approx 0$, survives for arbitrarily large values of μ, with κ showing a saturation behavior as in the 3-box case.

VI. MULTI-ANGLE STABILITY ANALYSIS

A. The consistency conditions

We now analyze how the single-angle picture of the instabilities is modified by the multi-angle effects. The linearization introduced in the paper allows our formalism to carry through to the multi-angle case.

The r.h.s. of the eigenvalue equation (41) is of the form $A+Bu$ where A and B are expressions that do not depend on either ω or u. So we are led to the ansatz

$$Q_{\omega,u} = \frac{a + b\,u}{\omega + u\bar{\lambda} - \Omega}\,, \tag{64}$$

where a and b are complex numbers. Inserting this ansatz provides

$$a + bu = \mu \int du'\, d\omega'\, g_{\omega',u'}\, \frac{(u+u')(a+b\,u')}{\omega' + u'\bar{\lambda} - \Omega}\,. \tag{65}$$

To understand better the structure of this equation, we define the integrals

$$I_n = \int du\, d\omega\, g_{\omega,u}\, \frac{u^n}{\omega + u\bar{\lambda} - \Omega}\,. \tag{66}$$

Then our eigenvalue equation becomes

$$a + bu = \mu\Big[(aI_1 + bI_2) + (aI_0 + bI_1)u\Big]\,. \tag{67}$$

If this is supposed to be true for every u we need to match the coefficients of the linear u polynomial on both sides separately. We can then write this in matrix form

$$\mu^{-1}\begin{pmatrix} a \\ b \end{pmatrix} = \begin{pmatrix} I_1 & I_2 \\ I_0 & I_1 \end{pmatrix}\begin{pmatrix} a \\ b \end{pmatrix}\,. \tag{68}$$

This has the form of an eigenvalue equation for a 2×2 matrix. This equation has nontrivial solutions if

$$\det\left[\begin{pmatrix} I_1 & I_2 \\ I_0 & I_1 \end{pmatrix} - \mu^{-1}\right] = 0 \tag{69}$$

or explicitly

$$\left(I_1 - \mu^{-1}\right)^2 = I_0 I_2 \,. \tag{70}$$

This is the multi-angle counterpart of our single-angle eigenvalue equation of Eq. (45).

B. Normal vs. inverted mass hierarchy

In the single-angle approximation, we saw that as far as the stability analysis is concerned, analysis of normal hierarchy is the same as that of the inverted one, except for a change of the sign of μ. This is true also in the multi-angle scenario, except that one also needs to change the sign of λ. Indeed, normal hierarchy changes Eq. (39) to

$$\begin{aligned} \mathrm{i}\partial_r \tilde{S}_{\omega,u} &= [-\omega + u(\lambda + \epsilon\mu)]\, \tilde{S}_{\omega,u} \\ &- \mu \int du'\, d\omega'\, (u + u')\, g_{\omega' u'}\, \tilde{S}_{\omega',u'} \,. \end{aligned} \tag{71}$$

The solution of this equation can be given in terms of the solution $S_{\omega,u}$ of Eq. (39) as

$$\begin{aligned} \tilde{S}_{\omega,u}(\mu, \lambda, g_{\omega,u}) &= S^*_{\omega,u}(\mu, -\lambda, -g_{\omega,u}) \\ &= S^*_{\omega,u}(-\mu, -\lambda, g_{\omega,u}) \,. \end{aligned} \tag{72}$$

Since S and S^* should have the same stability behavior, this implies that the stability conditions for normal hierarchy are the same as those for the inverted hierarchy with a change in the sign of g_ω or μ (not both at the same time), and an additional change in the sign of λ.

VII. MULTI-ANGLE STABILITY ANALYSIS: EXAMPLES

We now analyze the stability conditions with the multi-angle effects and compare them with our earlier results with single-angle approximation. We take the emission to be uniform over $0 \le u \le 1$. The integrals I_n can then be analytically calculated for the box spectra. The expressions, however, are not very illuminating, and we do not give them here. It turns out that the multi-angle effects modify the single-angle results in significant ways,

A. Two-box spectrum

The results of the multi-angle stability analysis of the two-box spectrum in the top panel of Fig. 2, in the absence of matter ($\lambda = 0$), are shown in the lower two panels. As far as the onset behavior is concerned, the multi-angle effects may be interpreted as some (complicated) average of the single-angle effects with different u_0 values. In particular, the value of κ at any value of μ lies within the range of κ for different u_0 values in the single-angle approximation. The comparison with a specific u_0 value ($u_0 = 1/2$) is shown in Fig. 5. As compared to this fixed value of u_0, the addition of multi-angle effects is observed to suppress the instability in some range of μ, while enhancing it at other values of μ.

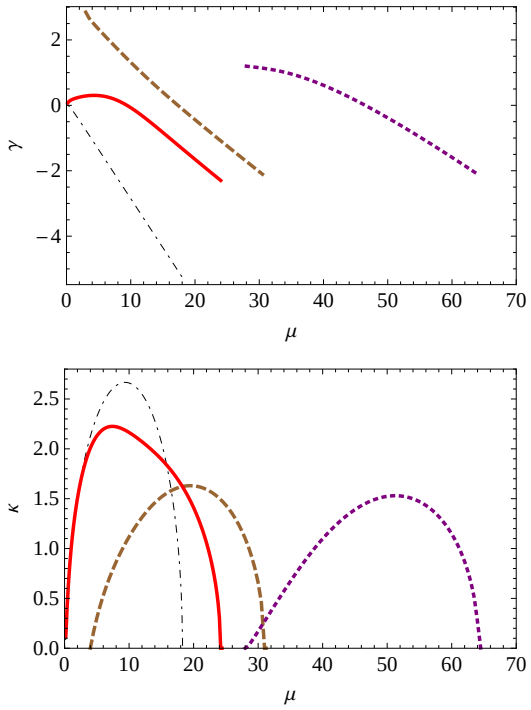

FIG. 5: The values of γ and κ for the two-box spectrum in Fig. 2, as a function of μ. Black (dash-dotted) line: single-angle approximation for $u_0 = 1/2$, red (solid) line: multi-angle effects with $\lambda = 0$, brown (dashed) line: multi-angle effects with $\lambda = 5$, purple (dotted) line: multi-angle effects with $\lambda = 30$,

The addition of finite matter effects shifts the range of μ where the instability occurs, to larger values of μ.

B. Three-box spectrum

The results of the multi-angle stability analysis of the three-box spectrum in the top panel of Fig. 3, in the absence of matter ($\lambda = 0$), are shown in the lower two panels. At low values of μ, the multi-angle affects may be interpreted as some (complicated) average of the single-angle effects with different u_0 values. At higher values of μ, though, the multi-angle effects are observed to suppress the instability as compared to the single-angle approximation. Most importantly, while the single-angle approximation showed a saturation behavior for all u_0 values, the multi-angle effects give rise to a threshold behavior. The comparison with a specific u_0 value

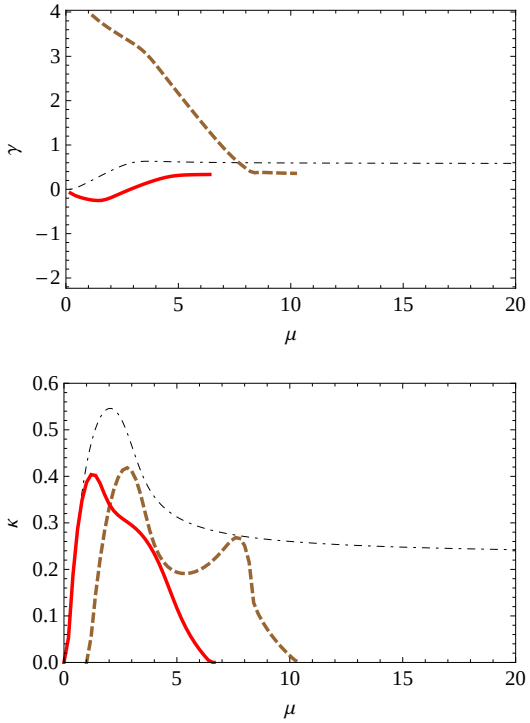

FIG. 6: The values of γ and κ for the three-box spectrum in Fig. 3, as a function of μ. Black (dash-dotted) line: single-angle approximation for $u_0 = 1/2$, red (solid) line: multi-angle effects with $\lambda = 0$, brown (dashed) line: multi-angle effects with $\lambda = 5$.

$(u_0 = 1/2)$ is shown in Fig. 6. As compared to this fixed value of u_0, the addition of multi-angle effects is observed to suppress the instability in some range of μ at some λ values (not shown in the figure), while enhancing it at other values of μ. At large μ values, the multi-angle effects always seem to suppress the instability. The addition of matter again shifts the instability region to higher values of μ.

C. A realistic SN spectrum

We now apply our stability analysis to a realistic SN spectrum, where the $(\nu_e, \bar{\nu}_e, \nu_x)$ spectra are taken to have the Fermi-Dirac form, with the temperatures $(2.1, 3.5, 4, 4)$ MeV and the chemical potentials $(3.9, 2.3, 2.1)$. These correspond to the average energies $(9.4, 13.0, 15.8)$ MeV. The ratio of number fluxes is taken to be $1.3 : 1.0 : 1.5$, where the total $\bar{\nu}_e$ flux is normalized to unity as per our normalization convention introduced in Sec. II A. This spectrum corresponds to the one recently studied in [27] for their multi-angle analysis including matter effects. We use $\Delta m^2 = (50\text{meV})^2$ in order to convert the energy scale to ω, which we show in the units of km^{-1}. The spectrum is shown in the top panel of Fig. 7.

The following observations may be made from the figure:

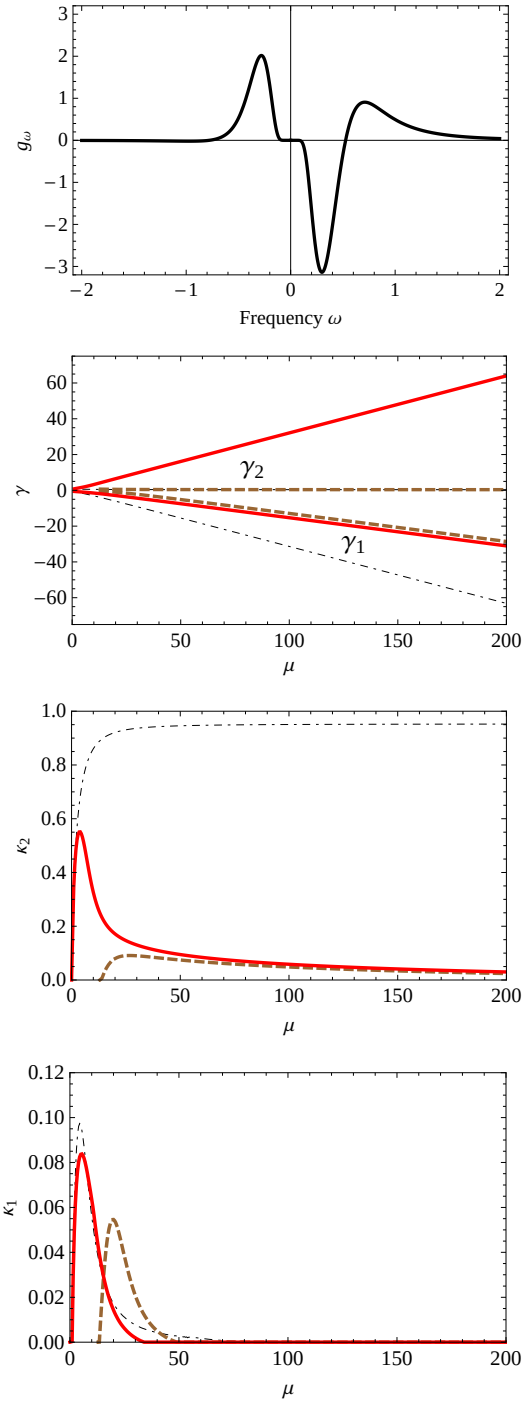

FIG. 7: The values of γ and κ as a function of μ, for the realistic SN spectrum in the top panel. Note that for $\omega < -0.8$, the value of g_ω is small and negative. The instability with higher γ is characterized by (γ_1, κ_1), while the other one is characterized by (γ_2, κ_2). Black (dash-dotted) line: single-angle approximation for $u_0 = 1/2$, red (solid) line: multi-angle effects with $\lambda = 0$, brown (dashed) line: multi-angle effects with $\lambda = 5$. Note that the scales for κ_1 and κ_2 are different.

- In the single-angle approximation, there are indeed two instabilities, centered approximately at the two positive zero-crossing points in the spectrum at very small values of μ. As μ increases, the centers of these instabilities (γ_1 and γ_2) move away from each other. The instability with the smaller γ shows a threshold-like behavior; it cannot show a perfectly threshold behavior since the spectrum does not identically vanish at large $|\omega|$. However the value of the corresponding κ goes to zero at large μ, so the effect of this instability will be very weak, almost imperceptible, at large μ. The other instability displays the saturation behavior: even at large μ, it has a nonzero κ value. This implies that, if the single-angle approximation is valid, there will be a strong instability however large the starting value of μ is. There is no synchronization phase.

- When multi-angle effects are added without ordinary matter ($\lambda = 0$), the effect is similar to the averaging of single-angle results, similar to that observed earlier in the two-box spectra. The instability is suppressed at large μ, through a threshold-like behavior. The other instability, which showed the saturation behavior with the single-angle approximation, now also shows the threshold-like behavior, i.e. the value of κ goes to zero at extremely large μ values. This however happens much more slowly as compared to the first instability, as can be seen in Fig. 7.

- The addition of matter effects shift the $\lambda = 0$ behavior to larger μ values, as was seen in the box-spectra examples we had studied earlier.

VIII. A NOVEL MULTI-ANGLE EFFECT

A surprising multi-angle result is obtained when $\bar{\lambda} = 0$, and the angular distribution is universal, i.e. $g_{\omega,u} = g_\omega f_u$, with $\int du f_u = 1$. Let us introduce the notation

$$G = \int d\omega \, \frac{g_\omega}{\omega - \Omega} \, . \tag{73}$$

Then in the multi-angle case, we have

$$I_n = G \int_0^1 du \, u^n = G \langle u^n \rangle \, . \tag{74}$$

The eigenvalue equation is then

$$\mu^{-1} = I_1 \pm \sqrt{I_0 I_2} = \left[\langle u \rangle \pm \langle u^2 \rangle^{1/2} \right] G \, . \tag{75}$$

The stability analysis then corresponds to determining the solutions $\Omega = \gamma \pm i\kappa$ for the equation

$$\mu^{-1} = \mathcal{K}_\pm G \, , \tag{76}$$

where $\mathcal{K}_\pm \equiv \langle u \rangle \pm \langle u^2 \rangle^{1/2}$.

In the single-angle approximation, $\langle u \rangle = u_0, \langle u^2 \rangle = u_0^2$, so that $\mathcal{K}_+ = 2u_0$ and $\mathcal{K}_- = 0$. The latter equation has no solution, since it would require $\mu^{-1} = 0$ identically. One may then write

$$\mu_{\rm single}^{-1} = 2u_0 G \, . \tag{77}$$

This may be solved to obtain the values of γ and κ in the single-angle approximation.

We can now write the two values of μ^{-1} in multi-angle analysis that correspond to the same values of γ and κ:

$$\mu_+^{-1} = \mathcal{K}_+ G \, , \quad \mu_-^{-1} = \mathcal{K}_- G \, , \tag{78}$$

Thus, there are two values of μ in multi-angle analysis that correspond to the same (γ, κ) in the single-angle analysis. The multi-angle stability behavior at these two μ values can then be understood by looking at the single-angle stability behavior at $\mu_{\rm single}$.

IX. SOLVING THE FULL NON-LINEAR EOMS FOR SINGLE CROSSED SPECTRUM

We now move away from the linearized onset regime, and look at the full non-linear EoM for the different modes. The non-linearity of the equations means that they are difficult to solve analytically, so we look for solutions in the simplest possible case. In this section, we consider a single-crossed spectrum, and also work with the single-angle assumption.

Following Eq(30), we define

$$\mathsf{S}_{\omega,r} = \begin{pmatrix} s_{\omega,r} & S_{\omega,r} \\ S^*_{\omega,r} & -s_{\omega,r} \end{pmatrix} \, . \tag{79}$$

for the single-angle case. Since S is a Hermitian 2×2 matrix, we can use Bloch vector decomposition and represent it by a vector. We choose a reference frame such that the z-component of the vector is given by $z = s_{\omega,r}$. We are still free to define our x and y-axes. One possible choice is to define $x = \Re(S)$ and $y = \Im(S)$. In this frame, the EoM's are given by

$$\dot{x} = -(\omega - \gamma) y + \mu z \int y g_\omega d\omega \tag{80}$$

$$\dot{y} = (\omega - \gamma) x - \mu z \int x g_\omega d\omega \tag{81}$$

$$\dot{z} = -\mu x \int y g_\omega d\omega \tag{82}$$

It turns out that the solutions are easier to find if we move to a frame rotating about the z-axis with a frequency such that $\int x g_\omega d\omega = 0$. In this frame

$$\dot{x} = -(\omega - \gamma) y + \mu z \int y g_\omega d\omega \tag{83}$$

$$\dot{y} = (\omega - \gamma) x \tag{84}$$

$$\dot{z} = -\mu x \int y g_\omega d\omega \, , \tag{85}$$

where

$$\gamma = -\mu \int z g_\omega d\omega + \frac{\int \omega y g_\omega d\omega}{\int y g_\omega d\omega} \,. \quad (86)$$

We try solutions of the form

$$x = -h_\omega \sin\phi \quad (87)$$
$$z = f_\omega \cos\phi + u_\omega \quad (88)$$

Substituting them back into Eqs.(83) and (85), we get the solutions to be

$$x = -\sin\phi f_\omega \quad (89)$$
$$y = \mu Y \frac{\omega-\gamma}{\kappa^2} f_\omega \quad (90)$$
$$z = \left(-\cos\phi + \frac{(\omega-\gamma)^2}{\kappa^2}\right) f_\omega \,, \quad (91)$$

where $Y = \int y g_\omega \, d\omega$, $\kappa^2 = \mu \int f_\omega(\omega-\gamma) g_\omega d\omega$, and f_ω is the normalization factor which turns out to be

$$f_\omega = \frac{\kappa^2}{\sqrt{(\omega-\gamma)^4 - 2(\omega-\gamma)^2\kappa^2\cos\phi_0 + \kappa^4}} \,. \quad (92)$$

We also derive the following conservation laws

$$\int d\omega \frac{g_\omega}{\sqrt{(\omega-\gamma)^4 - 2(\omega-\gamma)^2\kappa^2\cos\phi_0 + \kappa^4}} = 0 \quad (93)$$

$$\int d\omega \frac{(\omega-\gamma) g_\omega}{\sqrt{(\omega-\gamma)^4 - 2(\omega-\gamma)^2\kappa^2\cos\phi_0 + \kappa^4}} = \frac{1}{\mu} \quad (94)$$

$$\int d\omega \frac{(\omega-\gamma)^2 g_\omega}{\sqrt{(\omega-\gamma)^4 - 2(\omega-\gamma)^2\kappa^2\cos\phi_0 + \kappa^4}} = L \,, \quad (95)$$

where L is the lepton number. Note that Eqs. (93) and (94) are the same as Eqs. (46) and (47) when $\phi_0 = \pi$, whereas Eq. (95) says that lepton number is conserved in these oscillations.

X. ADIABATICALLY CHANGING BACKGROUND DENSITY

As the neutrinos emitted from the neutrinosphere stream out towards the surface of the supernova, the surrounding neutrino density begins to decrease with time. This means that the value of μ is now a monotonously decreasing function of time. It can be shown that the actual profile goes as $\mu(t) \propto t^{-4}$, but since we will work under the assumption that the change of μ is adiabatic, the explicit form of the time variation of μ turns out to be immaterial. In the last section, we have defined a parameter κ which is the frequency of collective oscillations. We can now define adiabaticity as the condition when $\kappa \gg \frac{\dot\mu}{\mu}$, which says that the internal time scale of the system is much faster than the time scale over which the external change, in this case the change in the value of μ, takes place. Under these conditions, we look for solutions such that they are perturbative corrections to the static solutions.

Let us assume that due to the change of μ with time, the solutions to the EOM's take the following form:

$$x = -\sin\phi f_\omega + A h_\omega \quad (96)$$
$$y = \mu Y \frac{\omega-\gamma}{\kappa^2} f_\omega + B h_\omega \quad (97)$$
$$z = \left(-\cos\phi + \frac{(\omega-\gamma)^2}{\kappa^2}\right) f_\omega + C h_\omega \quad (98)$$

where A, B, and C are independent of ω. The ω dependence of the new terms are all included in h_ω. Again substituting these forms back into the EoMs, and working at all times to first order in h_ω and time derivatives, we find that $h_\omega = \dot f_\omega$, $A = -\frac{3}{5}\frac{\mu Y}{\kappa^2}$, $B = 0$ and $C = -\frac{2}{5}\frac{\cos(\phi/2)}{\kappa}$. This means that there indeed exist solutions for adiabatically changing μ which are perturbations to the static μ solutions. The modified solutions for changing μ can now be written as

$$x = -\sin\phi f_\omega - \frac{3}{5}\frac{\mu Y}{\kappa^2}\dot f_\omega \quad (99)$$
$$y = \mu Y \frac{\omega-\gamma}{\kappa^2} f_\omega \quad (100)$$
$$z = \left(-\cos\phi + \frac{(\omega-\gamma)^2}{\kappa^2}\right) f_\omega - \frac{2}{5}\frac{\cos(\phi/2)}{\kappa}\dot f_\omega \quad (101)$$

We can also write down the equations of motion for ϕ and Y

$$\dot\phi = \mu Y \quad (102)$$
$$\dot Y = -\frac{\kappa^2}{\mu}\sin\phi + Y\left(-\frac{\dot\mu}{\mu} - \frac{6}{5}\frac{\dot\kappa}{\kappa} - \frac{11}{5}\frac{\dot\gamma}{\mu Z}\right) \quad (103)$$

The constraint equations, Eqs. (93-95), still hold at every point in time, with changing values of γ and κ (but with the same ϕ_0), as the value of μ goes from its initial value to 0 adiabatically.

XI. CONCLUSIONS

In this report, we have looked at two aspects of collective neutrino oscillations: how to describe the onset of these oscillations, and what the non-linear oscillations look like in simple cases. We briefly reviewed how interactions between neutrinos becomes important at high densities in supernovae. These interactions play a crucial role in collective oscillations which are not present otherwise. We have seen how these interactions lead to off-diagonal terms in the Hamiltonian written in the interaction basis. The presence of these terms couples the oscillations of all neutrinos and antineutrinos, and is the source of collective oscillations. Under the assumption

of azimuthal symmetry of neutrino radiation, we wrote down the effective Hamiltonian for the system. Using this, we were able to write down the linearized eigenvalue equation, which allowed us to describe an exponentially growing mode that would eventually develop into an instability.

We looked at the eigenvalue equation under the single-angle approximation and wrote down the consistency conditions which must be satisfied by the eigenvalues. Though all our analysis is done in the inverted hierarchy, we provided a prescription of how to look for instabilities in the system if we were working in the normal hierarchy. We then looked at toy examples where we could solve the constraint equations analytically and saw that various scenarios are possible. In the two-box spectra, we saw cutoff behavior of the roots, where the spectrum is stable beyond a certain value of μ. In the three-box case, we found that in certain spectra, it is also possible for the instability to persist even for arbitrarily large values of μ. From the four-box case we saw that two instabilities can start developing at the same time. In general, we saw that the number of instabilities is equal to the number of instable crossings in each hierarchy.

We then extended the linearization scheme to the full multi-angle case, and derived the consistency conditions for the same. Again, we provided a prescription of how to shift to the normal hierarchy from inverted hierarchy. We then looked again at the box spectra to see how the single-angle results were modified by the multi-angle analysis. We saw that while cutoff behavior of the roots persisted in multi-angle analysis, in some cases, saturation behavior also became cutoff behavior. We then looked at a realistic SN spectrum, which was studied in [27]. We found that the linearized analysis gave results consistent with the numerical results reported in the paper. The multi-angle analysis showed that the instabilities are suppressed as compared to the single-angle case.

The linearized multi-angle analysis gave a surprising result whereby it predicted that the two-box spectrum with a positive crossing and low lepton number can show collective oscillations in both normal and inverted hierarchy. However, this fact had been observed numerically in [25].

Whereas the linearized equations give us a handle to understand the onset of collective oscillations, it alone is not sufficient to understand the entire dynamical evolution of the oscillations. Therefore, we solved the full non-linear equation in the simplest case: a single crossed spectrum under the single-angle approximation. We found that the solutions can be written analytically and have the same form as the solutions of a pendulum. We then looked at the case when the background density of neutrinos changes adiabatically. We found that, in this case, there exist solutions which are perturbations about the steady state solutions. In theory, one could solve these equations and look at the evolution of the collective oscillations as the neutrinos stream out of the supernova. However, it turns out that this is not an easy task, and one must resort to numerical simulations.

[1] L. Wolfenstein, "Neutrino oscillations in matter," Phys. Rev. D **17**, 2369 (1978).

[2] S. P. Mikheev and A. Y. Smirnov, "Resonance enhancement of oscillations in matter and solar neutrino spectroscopy," Sov. J. Nucl. Phys. **42**, 913 (1985) [Yad. Fiz. **42**, 1441 (1985)].

[3] S. P. Mikheev and A. Y. Smirnov, "Neutrino oscillations in a variable density medium and neutrino bursts due to the gravitational collapse of stars," Sov. Phys. JETP **64**, 4 (1986) [Zh. Eksp. Teor. Fiz. **91**, 7 (1986)] [arXiv:0706.0454].

[4] A. S. Dighe and A. Y. Smirnov, "Identifying the neutrino mass spectrum from the neutrino burst from a supernova," Phys. Rev. D **62**, 033007 (2000) [hep-ph/9907423].

[5] T. K. Kuo and J. T. Pantaleone, "Neutrino oscillations in matter," Rev. Mod. Phys. **61**, 937 (1989).

[6] J. Pantaleone, "Neutrino oscillations at high densities," Phys. Lett. B **287**, 128 (1992).

[7] G. Sigl and G. Raffelt, "General kinetic description of relativistic mixed neutrinos," Nucl. Phys. B **406**, 423 (1993).

[8] S. Samuel, "Neutrino oscillations in dense neutrino gases," Phys. Rev. D **48**, 1462 (1993).

[9] V. A. Kostelecký and S. Samuel, "Neutrino oscillations in the early universe with an inverted neutrino mass hierarchy," Phys. Lett. B **318**, 127 (1993).

[10] V. A. Kostelecký and S. Samuel, "Self-maintained coherent oscillations in dense neutrino gases," Phys. Rev. D **52**, 621 (1995). [hep-ph/9506262].

[11] S. Samuel, "Bimodal coherence in dense selfinteracting neutrino gases," Phys. Rev. D **53**, 5382 (1996). [hep-ph/9604341].

[12] H. Duan, G. M. Fuller, J. Carlson and Y. Z. Qian, "Simulation of coherent non-linear neutrino flavor transformation in the supernova environment. I: Correlated neutrino trajectories," Phys. Rev. D **74**, 105014 (2006) [astro-ph/0606616].

[13] G. Raffelt and A. Yu. Smirnov, "Self-induced spectral splits in supernova neutrino fluxes," Phys. Rev. D **76**, 081301 (2007); Erratum ibid. **77**, 029903 (2008) [arXiv:0705.1830]; "Adiabaticity and spectral splits in collective neutrino transformations," Phys. Rev. D **76**, 125008 (2007) [arXiv:0709.4641].

[14] H. Duan, G. M. Fuller and Y. Z. Qian, "A simple picture for neutrino flavor transformation in supernovae," Phys. Rev. D **76**, 085013 (2007) [arXiv:0706.4293].

[15] G. L. Fogli, E. Lisi, A. Marrone and A. Mirizzi, "Collective neutrino flavor transitions in supernovae and the role of trajectory averaging," JCAP **0712**, 010 (2007) [arXiv:0707.1998].

[16] G. L. Fogli, E. Lisi, A. Marrone, A. Mirizzi and I. Tamborra, "Low-energy spectral features of supernova

(anti)neutrinos in inverted hierarchy," Phys. Rev. D **78**, 097301 (2008) [arXiv:0808.0807].

[17] B. Dasgupta, A. Dighe, G. Raffelt and A. Yu. Smirnov, "Multiple spectral splits of supernova neutrinos," Phys. Rev. Lett. **103**, 051105 (2009) [arXiv:0904.3542].

[18] H. Duan, G. M. Fuller and Y. Z. Qian, "Collective neutrino oscillations," Annu. Rev. Nucl. Part. Sci. **60**, 569 (2010).

[19] S. Hannestad, G. Raffelt, G. Sigl and Y. Y. Y. Wong, "Self-induced conversion in dense neutrino gases: Pendulum in flavor space," Phys. Rev. D **74**, 105010 (2006); Erratum ibid. **76**, 029901 (2007) [astro-ph/0608695].

[20] H. Duan, G. M. Fuller, J. Carlson and Y. Z. Qian, "Analysis of collective neutrino flavor transformation in supernovae," Phys. Rev. D **75**, 125005 (2007) [astro-ph/0703776].

[21] G. G. Raffelt, "N-mode coherence in collective neutrino oscillations," Phys. Rev. D **83**, 105022 (2011) [arXiv:1103.2891.

[22] S. Chakraborty, T. Fischer, A. Mirizzi, N. Saviano and R. Tomàs, "Analysis of matter suppression in collective neutrino oscillations during the supernova accretion phase," arXiv:1105.1130.

[23] B. Dasgupta, E. P. O'Connor and C. D. Ott, "The role of collective neutrino flavor oscillations in core-collapse supernova shock revival," arXiv:1106.1167.

[24] G. G. Raffelt and G. Sigl, "Self-induced decoherence in dense neutrino gases," Phys. Rev. D **75**, 083002 (2007) [hep-ph/0701182].

[25] A. Esteban-Pretel, S. Pastor, R. Tomàs, G. G. Raffelt and G. Sigl, "Decoherence in supernova neutrino transformations suppressed by deleptonization," Phys. Rev. D **76**, 125018 (2007) [arXiv:0706.2498].

[26] G. G. Raffelt, "Self-induced parametric resonance in collective neutrino oscillations," Phys. Rev. D **78**, 125015 (2008) [arXiv:0810.1407].

[27] H. Duan and A. Friedland, "Self-induced suppression of collective neutrino oscillations in a supernova," Phys. Rev. Lett. **106**, 091101 (2011) [arXiv:1006.2359].

[28] A. Esteban-Pretel, A. Mirizzi, S. Pastor, R. Tomàs, G. G. Raffelt, P. D. Serpico and G. Sigl, "Role of dense matter in collective supernova neutrino transformations," Phys. Rev. D **78**, 085012 (2008) [arXiv:0807.0659].

[29] R. F. Sawyer, "The multi-angle instability in dense neutrino systems," Phys. Rev. D **79**, 105003 (2009) [arXiv:0803.4319].

[30] A. D. Dolgov, "Neutrinos in the early universe," Sov. J. Nucl. Phys. **33**, 700 (1981) [Yad. Fiz. **33**, 1309 (1981)].